

GAMMA-RAY BURST IN A MOLECULAR CLOUD: DESTRUCTION OF DUST AND H₂ AND THE EMERGENT SPECTRUM

B. T. DRAINE AND LEI HAO

Princeton University Observatory, Peyton Hall, Ivy Lane, Princeton, NJ 08544; draine@astro.princeton.edu, haol@astro.princeton.edu
Received 2001 August 14; accepted 2002 January 1

ABSTRACT

A gamma-ray burst (GRB) with strong optical-UV emission occurring in a molecular cloud will photodissociate H₂, photoionize H₂, H, and He, and destroy dust grains. We model these processes, including time-dependent radiative transfer, in both continuum radiation and the resonance lines of H₂. The UV will pump H₂ into vibrationally excited levels. We calculate the absorption spectrum imprinted on radiation from the GRB at various times. In addition to the strong absorption lines of $v = 0$ H₂ at $\lambda < 1110$ Å due to cold ambient gas, we find that radiation reaching us from the GRB and its afterglow will show strong absorption lines due to vibrationally excited H₂ at 1110 Å $< \lambda < 1705$ Å. These absorption lines, if observed, would provide unequivocal evidence for the association of the GRB with molecular gas. Low-resolution spectra will exhibit conspicuous features due to clustering of individual lines; a list of the strongest such absorption features is given for the spectral resolution $R \approx 350$ characteristic of the grism on the *Swift* UV-optical telescope.

Subject headings: galaxies: ISM — gamma rays: bursts — ISM: clouds — ISM: molecules — molecular processes

1. INTRODUCTION

Gamma-ray bursts (GRBs) rank among the most dramatic, most energetic, and least understood celestial phenomena. Although at least some GRBs are now known to originate from cosmological distances, the progenitor objects, or their locations in galaxies, are not yet known. Only $\sim 40\%$ of GRBs have detectable optical afterglows, whereas the X-ray afterglow detection rate is $\sim 100\%$; the undetected optical afterglows may have been extinguished by dust in the host galaxy (see Lazzati, Covino, & Ghisellini 2002; Ramirez-Ruiz, Trentham, & Blain 2002, and references therein). Since GRBs may be associated with star-forming regions (Paczynski 1998, 2001; MacFadyen, Woosley, & Heger 2001), it is of interest to consider phenomena that would be indicative of molecular gas in the vicinity of the GRB.

At least some GRBs are accompanied by intense optical emission, as demonstrated by the detection of a 9th mag optical transient coinciding with GRB 990123 (Akerlof et al. 1999) and optical afterglows associated with other GRBs (e.g., GRB 990510; Stanek et al. 1999; Israel et al. 1999). The energy radiated in the optical-UV flash and afterglow can be substantial and can have dramatic effects on interstellar gas and dust in the vicinity of the GRB. The $h\nu > 13.6$ eV emission will photoionize the gas, and the pulse of optical radiation will vaporize dust grains out to substantial distances from the GRB (Waxman & Draine 2000, hereafter WD00). The gamma rays and hard X-rays emitted by the GRB will contribute to the ionization of the nearby gas, but the UV and soft X-rays have the dominant effect because of the much greater number of photons and much larger photoabsorption and photoionization cross sections. The time dependence of atomic and ionic absorption lines and photoionization edges in the spectra of GRBs has been discussed by Perna & Loeb (1998), Böttcher, Dermer, & Liang (1999), and Lazzati, Perna, & Ghisellini (2001). In this work, we focus on the rich absorption spectrum of H₂.

Ultraviolet radiation will destroy H₂ in the vicinity of the GRB, but before destruction, some of the H₂ molecules will be vibrationally excited by UV pumping. A preliminary study of the UV pumping (Draine 2000) found that high degrees of vibrational excitation would prevail in the H₂ undergoing photodissociation and photoionization, and an estimate of the column density of this vibrationally excited gas indicated that it could imprint a conspicuous absorption spectrum on light reaching us from the GRB flash and afterglow. If observed, this absorption at $\lambda \lesssim 1650$ Å would be a clear sign that the GRB was in close proximity to a molecular cloud.

The previous study did not explicitly include self-shielding in the H₂ lines or the details of the competition between the photoionization and photodissociation of H₂, and therefore it was only possible to make approximate estimates of the column density of vibrationally excited H₂. In this work, we carry out a detailed calculation of the effects of a high-luminosity optical transient on surrounding dust and molecular gas. We calculate the evolution of the dust and gas in the neighborhood of the source of radiation, including radiative transfer through the absorbing medium. We include the dominant sources of opacity: dust grains, H₂, H₂⁺, H, He, and He⁺. Computational limitations dictate using radial zones that can be optically thick to 13.6–100 eV ionizing photons and in the Lyman and Werner band transitions of H₂. We describe a numerical method that can be used to follow the motion of the ionization and dissociation fronts in this regime.

Our aim is to study the effects of the optical-UV transient for typical GRBs. At this time, our knowledge concerning the optical transients is extremely limited, with only one event (GRB 990123) observed near its peak brightness. Because GRB 990123 appears to have been unusually bright, in this paper we adopt a provisional model optical transient with a peak ultraviolet luminosity less than 1/40 that of GRB 990123 and an integrated optical luminosity per steradian perhaps 1% of GRB 990123. The GRB light

curve adopted for the calculation is given in § 2. The computational method is described in § 3, and the physical processes (dust destruction, photoexcitation, and photoionization) are summarized in § 4.

In § 6 we present results for our adopted light curve $L_\nu(t)$ for two cloud densities ($n_{\text{H}} = 10^3$ and 10^4 cm^{-3}) and for two different power-law indices ($\beta = -0.5$ and -1) for the UV–X-ray spectrum $L_\nu \propto \nu^\beta$. In § 7 we discuss the prospects for observing these absorption features in the spectrum of a GRB fireball or afterglow, either with ground-based observations of GRBs at redshift $z > 1.25$ or using the grism on the *Swift* GRB Explorer for GRBs at redshift $z > 0.06$. We summarize our results in § 8.

2. THE OPTICAL-UV FLASH

Let $L \equiv 4\pi dP/d\Omega$ where $dP/d\Omega$ is the radiated power per solid angle in our direction. It is not yet known what should be taken for the “typical” $L(t)$ for a GRB at optical–soft X-ray wavelengths.

In Figure 1 we show $\nu L_\nu(t)$ of GRB 990123 at redshift $z = 1.6$, at rest-frame wavelength $\sim 2000 \text{ \AA}$. As a simple fitting function to describe the time-dependent luminosity, we adopt

$$\nu L_\nu = L_0 \frac{4(t/t_0)^2}{[1 + (t/t_0)^2]^2} \left(\frac{h\nu}{13.6 \text{ eV}} \right)^{1+\beta}. \quad (1)$$

A spectral index $\beta = -0.5$ is suggested by simple models for the reverse shock (WD00). Steeper spectral indices have

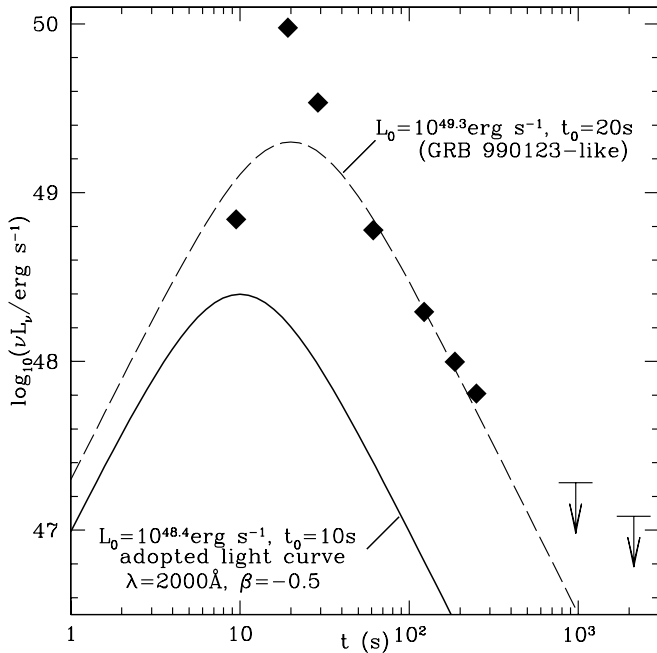


FIG. 1.—*Filled symbols*: Observed light curve of GRB 990123 (Akerlof et al. 1999) at $\lambda \approx 2000 \text{ \AA}$ in the rest frame (assuming $H_0 = 65 \text{ km s}^{-1} \text{ Mpc}^{-1}$, an open cosmology with $\Omega = 0.3$, and zero extinction). *Dashed curve*: Eq. (1) with $L_0 = 2 \times 10^{49} \text{ ergs s}^{-1}$ and $t_0 = 20 \text{ s}$. This underestimates the energy in the optical transient of GRB 990123. *Solid curve*: Eq. (1) with $L_0 = 2.5 \times 10^{48} \text{ ergs s}^{-1}$ and $t_0 = 10 \text{ s}$, which we adopt as a model for the optical transient.

been observed for optical-UV afterglows: for GRB 010222 at redshift $z \geq 1.475$ (Masetti et al. 2001), Lee et al. (2001) find $\beta = -0.90$ at $(1+z)t = 1.7 \times 10^4 \text{ s}$, Stanek et al. (2001) find $\beta = -1.07$ at $(1+z)t = 1.7 \times 10^4 \text{ s}$, and Masetti et al. (2001) find $\beta = -0.55$ for $8 \times 10^4 \text{ s} \lesssim (1+z)t \lesssim 1.6 \times 10^5 \text{ s}$.

With $L_0 = 2 \times 10^{49} \text{ ergs s}^{-1}$, $t_0 = 20 \text{ s}$, and $\beta \approx -0.5$, equation (1) approximates the light curve of GRB 990123 at $50 \text{ s} \lesssim t \lesssim 500 \text{ s}$, although falling at least a factor of 5 below the observed peak brightness at $t = 20 \text{ s}$ (see Fig. 1).

The $L_\nu \propto t^{-2}$ dependence of equation (1) at $t \gg t_0$ is required to approximate the observed rapid decline in brightness of GRB 990123 between 20 and 300 s (see Fig. 1). However, at later times, afterglows appear to fade less rapidly: for GRB 010222, $L_\nu \propto t^{-0.75 \pm 0.05}$ for $1.7 \times 10^4 \text{ s} \lesssim (1+z)t \lesssim 3 \times 10^4 \text{ s}$ and $L_\nu \propto t^{-1.3}$ for $8 \times 10^4 \text{ s} \lesssim (1+z)t \lesssim 3 \times 10^6 \text{ s}$ (Stanek et al. 2001; Masetti et al. 2001). For the present study, we are concerned with the light curve at $t \lesssim 10^3 \text{ s}$, which we approximate using equation (1).

GRB 990123 was in the top 0.4% in gamma-ray fluence for GRBs detected by the BATSE instrument, and Livermore Optical Transient Imaging System (LOTIS) observations further suggest that most GRBs detected by BATSE have lower ratios of optical-to-gamma-ray emission (Williams et al. 2000). Accordingly, we adopt $L_0 = 2.5 \times 10^{48} \text{ ergs s}^{-1}$, i.e., a peak luminosity of about 1/40 of what was observed for GRB 990123, and $t_0 \approx 10 \text{ s}$ as “typical” parameters. For $\beta = -0.5$, this corresponds to the optical transient having an energy between 1 and 13.6 eV, given by $E_{\text{OT}} = 2\pi L_0 t_0 (\Omega/4\pi) [1 - (1/13.6)^{1+\beta}] / (1+\beta) = 1.57 \times 10^{50} (\Omega/4\pi) \text{ ergs}$; for $\beta = -1$, $E_{\text{OT}} = 2\pi L_0 t_0 (\Omega/4\pi) \ln 13.6 = 4.1 \times 10^{50} (\Omega/4\pi) \text{ ergs}$, where $\Omega/4\pi$ is the beaming fraction.

The propagation of the dust-destruction, photodissociation, and photoionization fronts will of course depend on the adopted luminosity of the optical transient and on its spectrum. We consider our provisional light curve to be reasonable given present uncertainties. Because the medium is (at least initially) extremely optically thick, with dust destruction furthermore depending nonlinearly on the radiation intensity, there are no simple scaling relations for the solutions, but an increase or decrease in the adopted luminosity will of course result in an increase or decrease in the front propagation speeds. Because dust destruction is nonlinear, changes in the luminosity can have a larger effect on the speed of the dust-destruction front than on the speed of the photoionization/dissociation fronts.

3. RADIATIVE TRANSFER

We divide the cloud into spherical shells $j = 1, \dots, N$ of uniform thickness ΔR , with outer radii R_j and midpoints $\bar{R}_j \equiv R_j - 0.5 \Delta R$. At each radius r , let $t_r \equiv t - r/c$ be the “retarded” time.

The shell thickness ΔR is small enough ($n_{\text{H}} \Delta R < 10^{21} \text{ cm}^{-2}$) that an individual shell is optically thin in dust, but the shells may be optically thick to photoionizing radiation or in absorption lines of H_2 . We therefore calculate rates for photoionization, photodissociation, or photoabsorption averaged over the shell volume

$$\Delta V_j \equiv (4\pi/3) [R_j^3 - (R_j - \Delta R)^3]. \quad (2)$$

At frequency ν , the optical depth contributed by shell j is

$$\Delta\tau_j(\nu) \equiv \delta\tau_{d,j}(\nu) + \delta\tau_{\text{H}_2,j}(\nu) + \delta\tau_{\text{H}_2^+,j}(\nu) + \delta\tau_{\text{H},j}(\nu) \\ + \delta\tau_{\text{He}^0,j}(\nu) + \delta\tau_{\text{He}^+,j}(\nu) + \sum_{\alpha}' \delta\tau_{\alpha,j}(\nu), \quad (3)$$

where $\delta\tau_{d,j}$, $\delta\tau_{\text{H}_2,j}$, $\delta\tau_{\text{H}_2^+,j}$, $\delta\tau_{\text{H},j}$, $\delta\tau_{\text{He}^0,j}$, and $\delta\tau_{\text{He}^+,j}$ are the contributions in shell j due to extinction by dust, and continuous absorption by H_2 , H_2^+ , H , He^0 , and He^+ , respectively; $\delta\tau_{\alpha,j}$ is the contribution of an individual H_2 absorption line α (see § 3.3). Absorption by metals not in dust grains (initially, O, N, Ne, and S will be most important, and C, Mg, Si, and Fe will enter the gas phase in regions where grains are vaporized) has been neglected in equation (3), because the present calculation is limited to the gas-phase species H, H^+ , H_2 , H_2^+ , He, He^+ , and He^{2+} . We have thereby underestimated the attenuation at $h\nu \gtrsim 100$ eV.

We divide the electromagnetic spectrum into three intervals: $h\nu < 11.1$ eV, 11.1 eV $< h\nu < 13.6$ eV, and 13.6 eV $< h\nu < 20$ keV. For purposes of modeling the heating of dust grains by the UV-optical radiation, we include the contribution of H_2 absorption lines only within the interval 11.1 eV $< h\nu < 13.6$ eV; the summation \sum' in equation (3) is restricted to lines α within this interval, with $\delta\tau_{\alpha}$ calculated from equation (15) below.

The total optical depth from $r = 0$ to R_j is

$$\tau_j(\nu, t_r) = \sum_{i=1}^j \Delta\tau_i(\nu, t_r). \quad (4)$$

3.1. Absorption and Scattering by Dust

The contribution by the dust in shell j is

$$\delta\tau_{d,j}(\nu) = n_{d,j} \pi a_j^2 [Q_{\text{abs}}(\nu) + Q_{\text{sca}}(\nu)] \Delta R, \quad (5)$$

where $a_j(t_r)$ is the dust radius in shell j at retarded time t_r , and $Q_{\text{abs}}(\nu)$ and $Q_{\text{sca}}(\nu)$ are the usual efficiency factors for absorption and scattering. The radiation from the GRB is concentrated in a shell-like pulse with a spatial thickness of ~ 10 lt-s (see Fig. 1). Scattering is important because it reduces the intensity in the pulse; the scattered photons will fall behind the outward-propagating pulse unless the scattering angle is very small. For scattering angle $\theta \ll 1$, after travelling a distance δR , a scattered photon will fall behind the unscattered pulse by a time

$$\delta t \approx \frac{\delta R \theta^2}{2c} = (1.4 \text{ s}) \frac{\delta R}{10^{18} \text{ cm}} \left(\frac{\theta}{\text{arcmin}} \right)^2, \quad (6)$$

so that the time delay will be significant for scattering angle $\theta \gtrsim 5'$. The dust grains will have radii $a \approx 3 \times 10^{-5}$ cm (see § 5.1). For $a = 0.25 \mu\text{m}$, the characteristic scattering angle is $\sim 3'$ at 2 keV, and $\sim 10'$ at 0.5 keV (see Figs. 3 and 4 of Smith & Dwek 1998), so we take the scattering efficiency factor to be

$$Q_{\text{sca}}(\nu) = \begin{cases} 0 & h\nu < 1 \text{ eV}, \\ 1 & 1 \text{ eV} \leq h\nu < 1 \text{ keV}, \\ 0 & h\nu \geq 1 \text{ keV}. \end{cases} \quad (7)$$

In Figure 2 we show Q_{abs} calculated for $a = 0.3 \mu\text{m}$ graphite and silicate grains. At $h\nu \gtrsim 1$ keV, the silicate absorption efficiency is much larger because of the inner-shell absorp-

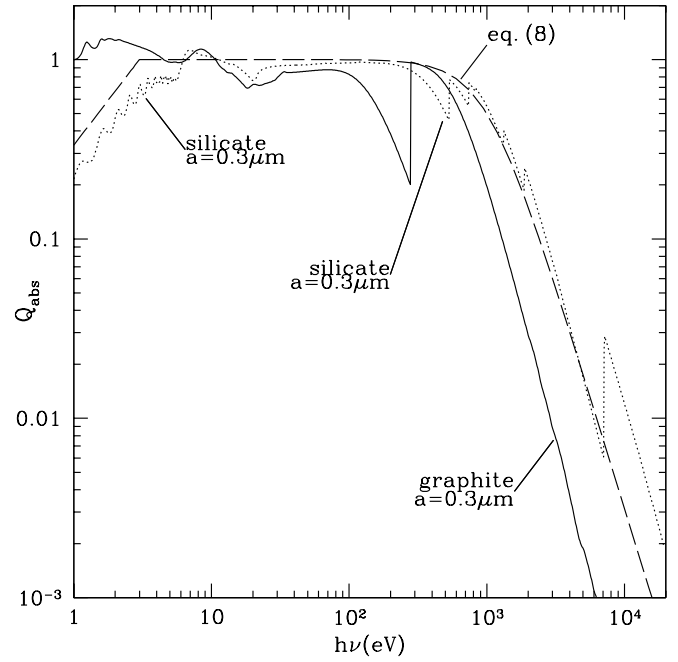


FIG. 2.—Absorption efficiency Q_{abs} for $a = 0.3 \mu\text{m}$ radius graphite and silicate grains.

tions from Mg, Si, and Fe. In the present calculation, we do not distinguish between grain types, and we need a simple estimate for the absorption efficiency that can be rapidly evaluated. As a simple approximation, we adopt

$$Q_{\text{abs}}(\nu) = \begin{cases} h\nu/(3 \text{ eV}) & h\nu < 3 \text{ eV}, \\ 1/[1 + (h\nu/\text{keV})^{2.5}] & h\nu \geq 3 \text{ eV}, \end{cases} \quad (8)$$

which can be seen in Figure 2 to provide a reasonable approximation to the average absorption cross sections of graphite and silicate grains, although at energies $100 \text{ eV} < h\nu < 250 \text{ eV}$ and $h\nu \gtrsim 700 \text{ eV}$, the carbonaceous grains are considerably less absorptive. In our simulations, the dust-destruction front quickly moves ahead of the ionization front, so that $h\nu > 13.6$ eV ionizing photons make only a minor contribution to grain heating.

When grain destruction has reduced the grain radius to $a \ll 3 \times 10^{-5}$ cm, equation (8) will overestimate Q_{abs} ; when this is true, however, grain destruction is nearly complete and the error in overall grain destruction will be unimportant.

3.2. Continuous Absorption by Atoms, Molecules, and Ions

Continuous absorption by species X contributes

$$\delta\tau_{X,j}(\nu) = n_{X,j} \Delta R \sigma_X(\nu), \quad (9)$$

where $n_{X,j}(t_r)$ is the abundance of X in shell j at retarded time t_r , and $\sigma_X(\nu)$ is the continuous absorption cross section.

The probability that a photon that enters the shell will be absorbed or scattered is $(1 - e^{-\Delta\tau_j})$. For a homogeneous shell, a fraction $\delta\tau_{X,j}/\Delta\tau_j = n_{X,j}\sigma_X \Delta R/\Delta\tau_j$ will be due to continuous absorption by species X (e.g., $X + h\nu \rightarrow X^+ + e^-$). The photon absorption rate per X,

averaged over the shell, is

$$\zeta_X = \frac{\Delta R}{\Delta V_j} \int_{\nu_X}^{\infty} \frac{L_\nu d\nu}{h\nu} e^{-\tau_j} \frac{(1 - e^{-\Delta\tau_j})}{\Delta\tau_j} \sigma_X(\nu). \quad (10)$$

Integration over frequency ν is accomplished numerically, with $\Delta\tau_j$ and τ_{j-1} evaluated using equations (3) and (4).

3.3. Line Absorption

Line absorption is important for H_2 . Consider a specific absorption line α , with central frequency ν_α . We assume that the H_2 has a Maxwellian velocity distribution with broadening parameter b , and we compute the dimensionless equivalent width

$$W_\alpha(R_j) = \int \frac{d\nu}{\nu} \{1 - \exp[-N_\alpha(R_j)\sigma_\alpha(\nu)]\}, \quad (11)$$

where $\sigma_\alpha(\nu)$ is the (Voigt profile) absorption cross section for absorption line α and

$$N_\alpha(R_j) = \sum_{i=1}^j n_{\alpha,i} \Delta R \quad (12)$$

is the column density of the vibration-rotation state (v_α, J_α) producing absorption line α .

The column density and incremental equivalent width contributed by shell j are

$$\delta N_{\alpha,j} = N_\alpha(R_j) - N_\alpha(R_{j-1}) = n_{\alpha,j} \Delta R, \quad (13)$$

$$\delta W_{\alpha,j} = W_\alpha(R_j) - W_\alpha(R_{j-1}). \quad (14)$$

If we approximate the line absorption as due to many lines randomly distributed over the frequency interval $[\nu_{\min}, \nu_{\max}]$, the optical depth contribution due to line α averaged over the wavelength interval is (see Draine & Bertoldi 1996)

$$\delta\tau_{\alpha,j} = \frac{\delta W_{\alpha,j}}{\ln(\nu_{\max}/\nu_{\min})} \quad \text{for } \nu_\alpha \in [\nu_{\min}, \nu_{\max}], \quad (15)$$

and the mean photoabsorption rate in radial shell j for excitation out of level X_α by the absorption line α is obtained by dividing the rate of line absorptions in shell j by the number of molecules $4\pi\bar{R}_j^2\delta N_{\alpha,j}$ in level α in shell j :

$$\zeta_{X_{\alpha,j}} = L_\nu e^{-\tau_{j-1}} \frac{\delta W_{\alpha,j}}{4\pi\bar{R}_j^2 \delta N_{\alpha,j} h}. \quad (16)$$

Strong line absorption by H_2 occurs primarily in $[h\nu_{\min}, h\nu_{\max}] = [11.2, 13.6]$ eV, so we include the optical depth correction from equation (15) for this interval only.

4. PHYSICAL PROCESSES

4.1. Dust Destruction by Thermal Sublimation

The thermal sublimation rate from a grain at temperature T can be approximated by (Guhathakurta & Draine 1989, hereafter GD89)

$$\frac{da}{dt} = -\left(\frac{m}{\rho}\right)^{1/3} \nu_0 e^{-B/kT}, \quad (17)$$

where m is the mean atomic mass and B is the chemical binding energy per atom. We take $\nu_0 = 1 \times 10^{15} \text{ s}^{-1}$,

$B/k = 7 \times 10^4 \text{ K}$, and $\rho/m = 1 \times 10^{23} \text{ cm}^{-3}$ as representative values for refractory grains (GD89; WD00). We assume that all of the energy of absorbed photons (including X-rays) is converted to heat—we neglect the energy of photoelectrons and X-ray fluorescence, but this is a small fraction of the total absorbed energy.

In the middle of shell j , the grain temperature T is determined by (WD00)

$$\int_0^\infty \frac{L_\nu d\nu}{4\pi\bar{R}_j^2} \exp(-\tau_{\nu,j-1} - 0.5\Delta\tau_{\nu,j}) Q_{\text{abs}} \pi a^2 = \langle Q \rangle_T 4\pi a^2 \sigma T^4 - 4\pi a^2 \frac{da}{dt} \frac{\rho}{m} B, \quad (18)$$

where $\langle Q \rangle_T$ is the Planck-averaged absorption efficiency. For the temperature range of interest for dust sublimation, $2000 \text{ K} \lesssim T \lesssim 3000 \text{ K}$, we approximate (WD00)

$$\langle Q \rangle_T \approx \frac{0.1(a/10^{-5} \text{ cm})(T/2300 \text{ K})}{1 + 0.1(a/10^{-5} \text{ cm})(T/2300 \text{ K})}, \quad (19)$$

intermediate between the emissivities of astronomical silicate and graphite.

4.2. Dust Destruction by Electrostatic Stresses?

WD00 noted that a highly charged dust grain can also be destroyed by ‘‘Coulomb explosion’’ if the electrostatic stress exceeds the tensile strength of the grain materials, when the grain potential reaches

$$U_{\text{frac}} \approx (3000 \text{ V})(S_{\text{max}}/10^{11} \text{ dyn cm}^{-2})^{1/2}(a/10^{-5} \text{ cm}). \quad (20)$$

The importance of this process is uncertain. Waxman & Draine argued that submicron grains would likely have high enough tensile strengths ($S_{\text{max}} > 1 \times 10^{11} \text{ dyn cm}^{-2}$) that highly charged grains would not undergo fission by this process, but would instead be gradually eroded by the process of ‘‘ion field emission,’’ in which singly charged ions are emitted one by one when the grain potential exceeds a critical value

$$U_{\text{IFE}} \approx (3 \times 10^3 \text{ V})(a/10^{-5} \text{ cm}) \quad (21)$$

(Muller & Tsong 1969; Draine & Salpeter 1979). Fruchter, Krolik, & Rhoads (2001), on the other hand, have argued for lower tensile strengths ($S_{\text{max}} \approx 10^{10} \text{ dyn cm}^{-2}$), in which case grain fission would take place when the grain potential reached $U_{\text{frac}} \approx (950 \text{ V})(a/10^{-5} \text{ cm})(S_{\text{max}}/10^{10} \text{ dyn cm}^{-2})^{1/2}$. Fruchter et al. argue that ‘‘the large flux of energetic photons bombarding the grain is likely to damage the grain’s crystalline structure,’’ reducing the tensile strength.

While chemical bonds will undoubtedly be disrupted by ionization, it seems likely that chemical bonds will be promptly reestablished in the warm grain, i.e., ‘‘annealing’’ will take place. In this case, a grain that has already been charged to the ion-field emission threshold potential U_{IFE} would emit one ion per escaping photoelectron. To sustain ion field emission, the grain must emit photoelectrons with sufficient energy to overcome the potential $U_{\text{IFE}} = (3000 \text{ V})(a/10^{-5} \text{ cm})$. Consider, for example, a grain with radius $a = 3 \times 10^{-5} \text{ cm}$, charged to $U_{\text{IFE}} \approx 9 \text{ kV}$: only photoelectrons with kinetic energy at the grain surface $E > eU \approx 9 \text{ keV}$ are able to escape. For a grain with com-

position MgFeSiO_4 , a photon of energy $h\nu = 10$ keV (for example) has a total absorption coefficient $\alpha = 600 \text{ cm}^{-1}$ in the grain material, but only $\sim 4\%$ of the absorptions produce photoelectrons with $E > 9$ keV,¹ for an effective absorption coefficient of 24 cm^{-1} . The total electron density in the grain is $1 \times 10^{24} \text{ cm}^{-3}$, so the effective photoionization cross section per electron is $\sim 24 \times 10^{-24} \text{ cm}^2$ —a factor of 24 larger than estimated by WD00.

Grain destruction by ion field emission requires a fluence $F_{\text{IFE}} \approx (\rho/m)/\alpha_{\text{IFE}}$, where $\rho/m \approx 10^{23} \text{ cm}^{-3}$ is the atomic density and α_{IFE} is the effective absorption coefficient for producing photoelectrons with energies greater than eU_{IFE} . For $U_{\text{IFE}} = 9$ kV, we have $\alpha_{\text{IFE}} = 24 \text{ cm}^{-1}$ and $F_{\text{IFE}} = 4 \times 10^{21} \text{ cm}^{-2}$ of $h\nu \gtrsim 10$ keV photons. For $\beta = -0.5$ and distance D , the fluence of $h\nu > 10$ keV photons is $2.2 \times 10^{21} (L_0 t_0 / 10^{49.4} \text{ ergs})(\text{pc}/D)^2 \text{ cm}^{-2}$ (neglecting absorption), so we might expect grain destruction by ion field emission at distances $D \lesssim 1$ pc. However, as we see below (§ 6), grain destruction by thermal sublimation is effective out to distances of several parsecs. If grains have tensile strengths $S_{\text{max}} \lesssim 10^{10} \text{ cm}^{-2}$, as argued by Fruchter et al. (2001), then X-ray photoelectric emission can lead to grain fission by Coulomb explosions out to even greater distances.

4.3. Photoexcitation of H_2

Let index $i = 1, \dots, N$ denote the vibration-rotation levels of the electronic ground state $X^1\Sigma_g^+$. At a given point in the cloud, let $p_i(t) \equiv 2n(\text{H}_2(v_i, J_i))/n_{\text{H}}$ be the fraction of H nuclei that are in vibration-rotation level i .

Prior to the GRB, H_2 is almost entirely in the first two or three rotational levels ($J = 0, 1, 2$) of the $v = 0$ vibrational level of the electronic ground state ($X^1\Sigma_g^+$). The first UV photons to be absorbed will photoexcite the H_2 to the $B^1\Sigma_u^+$ and $C^1\Pi_u^+$ electronic states (via Lyman or Werner band transitions), which requires $h\nu > 11.2$ and 12.3 eV, respectively, or photoionize the H_2 to H_2^+ , which requires $h\nu > 15.4$ eV [for $\text{H}_2(v = 0)$]. The H_2 that is photoexcited to the B or C states will decay back to the ground electronic state in $\sim 10^{-9}$ s, but typically to a vibrationally excited level (e.g., $v = 5$) with the rotational quantum number changed by $\Delta J = 0, \pm 2$. The lifetimes of the vibrationally excited levels are long compared to the timescale for photoexcitation or photoionization, so depopulation of the vibrationally excited levels of H_2 will be primarily by UV photoexcitation and photoionization.

The intensity of the radiation field at 1000 \AA relative to the local interstellar radiation field estimate of Habing (1968) is

$$\begin{aligned} \chi &= \frac{(\nu u_\nu)_{1000 \text{ \AA}}}{4 \times 10^{-14} \text{ ergs cm}^{-3}} \\ &= 7 \times 10^{12} \frac{\nu L_\nu}{10^{48} \text{ ergs s}^{-1}} \left(\frac{\text{pc}}{R}\right)^2 \exp[-\tau(1000 \text{ \AA})]. \quad (22) \end{aligned}$$

Stimulated emission in the UV transitions is negligible if $\chi \ll 10^{19}$. We therefore assume that photoexcitation out of level i of $X^1\Sigma_g^+$ to vibration-rotation states of $B^1\Sigma_u^+$ and $C^1\Pi_u^+$ will be followed (immediately) by spontaneous decay either to bound levels j of the ground electronic state $X^1\Sigma_g^+$ or else to the vibrational continuum of $X^1\Sigma_g^+$ (i.e., photo-

dissociation). The H_2 formation on grains or in the gas is neglected, since we are concerned with conditions in which the H_2 is destroyed in a matter of seconds or minutes. Collisional deexcitation can be neglected if $n_{\text{H}}/\text{cm}^{-3} \ll \chi$. The spontaneous decay via quadrupole transitions out of vibrationally excited level i can also be neglected if $\chi \gg 10^4$.

Let T_{ji} be the rate for the photopumping of H_2 out of level i into level j , and let $\zeta_i^{(\text{pd})}$ and $\zeta_i^{(\text{pi})}$ be the rates for photodissociation and photoionization out of level i . If

$$T_{ii} \equiv - \left(\sum_{j \neq i} T_{ji} + \zeta_i^{(\text{pd})} + \zeta_i^{(\text{pi})} \right), \quad (23)$$

then the H_2 abundances $p_i \equiv 2n(\text{H}_2(v_i, J_i))/n_{\text{H}}$ evolve according to

$$\frac{dp_i}{dt} = \sum_j T_{ij} p_j. \quad (24)$$

Following Draine & Bertoldi (1996), we consider the 299 bound states of H_2 with $J \leq 29$ and calculate equivalent widths W_α using Lyman and Werner band oscillator strengths from Abgrall et al. (1993a, 1993b) and E. Roueff (1993, private communication).

Let α denote a Lyman or Werner band transition from a specific vibration-rotation state i of the electronic ground state to an excited state $u(\alpha)$. Photoexcitation rates ζ_α in shell j are calculated using equation (16). Let $P_{j,u}$ be the probability that electronically excited state u will decay to vibration-rotation state j of the electronic ground state. Averaged over the shell, the rate for UV pumping from vibration-rotation level i to vibration-rotation level j is

$$T_{ji} = \sum_\alpha' P_{j,u(\alpha)} \zeta_\alpha, \quad (25)$$

where the summation is restricted to transitions α out of level i . The photodissociation rate out of level i is

$$\zeta_i^{(\text{pd})} = \sum_\alpha' p_{\text{diss}}(u(\alpha)) \zeta_\alpha, \quad (26)$$

where $p_{\text{diss}}(u)$ is the probability that level u will decay by a transition to the vibrational continuum.

The first electronic excited state of the H_2^+ ion has only three weakly bound vibration-rotation states, and transitions from the ground state to higher states have unfavorable Franck-Condon factors (Leach & Moss 1995). Hence, H_2^+ photoabsorptions are expected to be mainly in transitions to the photodissociation continuum ($\text{H}_2^+ + h\nu \rightarrow \text{H}^+ + \text{H}$; see § 4.5 below) and photoionization ($\text{H}_2^+ + h\nu \rightarrow 2\text{H}^+ + e^-$; see § 4.6 below). We therefore neglect line absorption by H_2^+ .

4.4. $\text{H}_2 + h\nu \rightarrow \text{H}_2^+ + e^-$

The different vibration-rotation levels of the electronic ground state of H_2 will have different energy thresholds for photoionization. However, we neglect these differences and assume that all H_2 in the ground electronic state requires $h\nu > 15.4$ eV to be photoionized, with the cross section as given by equations (17)–(19) of Yan, Sadeghpour, & Dalgarno (1998). The photoionization rate $\zeta_{\text{H}_2}^{(\text{pi})}$ averaged over the shell is evaluated using equation (10).

¹ Photons of $h\nu = 10$ keV absorbed by the Mg, Si, and Fe K shells (with photoelectric thresholds $E_T = 1.32, 1.87,$ and 7.11 keV) produce photoelectrons with $h\nu - E_T = 8.68, 8.13,$ and 2.89 keV, respectively.

4.5. $\text{H}_2^+ + h\nu \rightarrow \text{H}^+ + \text{H}$

H_2^+ has 19 vibrational levels; for photoionization of $\text{H}_2^+(v=0)$, the H_2^+ vibrational distribution is expected to peak at $v=2$, with 80% of the population in $v \leq 5$ (von Busch & Dunn 1972). With radiative lifetimes of $\sim 10^7$ s, there will be negligible deexcitation by spontaneous decay during the optical transient. Averaged over the H_2^+ vibrational distribution, the photodissociation cross section found by von Busch & Dunn (1972) can be fit by

$$\sigma = (2.7 \times 10^{-16} \text{ cm}^2) \left(\frac{h\nu}{29 \text{ eV}} \right)^2 \left(1 - \frac{h\nu}{29 \text{ eV}} \right)^6$$

for $h\nu < 29 \text{ eV}$, (27)

giving a peak cross section $\sigma \approx 3 \times 10^{-18} \text{ cm}^2$ at $h\nu \approx 7.3 \text{ eV}$ ($\lambda \approx 1700 \text{ \AA}$). The photodissociation rate $\zeta_{\text{H}_2^+}^{(\text{pd})}$ averaged over the shell is evaluated using equation (10).

4.6. $\text{H}_2^+ + h\nu \rightarrow 2\text{H}^+ + e^-$

For photoionization of H_2^+ , we adopt a cross section

$$\sigma = 9.3 \times 10^{-19} \text{ cm}^2 \left(\frac{h\nu}{15.4 \text{ eV}} \right)^{-2} \quad \text{for } h\nu > 15.4 \text{ eV},$$

(28)

which approximates the photoionization cross section calculated by Bates & Öpik (1968) for the ground vibrational state of $\text{H}_2^+(v=0)$. The photoionization rate $\zeta_{\text{H}_2^+}^{(\text{pi})}$ averaged over the shell is evaluated using equation (10).

4.7. $\text{H} + h\nu \rightarrow \text{H}^+ + e^-$

Atomic H from the photodissociation of H_2 or H_2^+ can be photoionized by photons with $h\nu > I_{\text{H}} = 13.6 \text{ eV}$ with a cross section (Osterbrock 1989)

$$\sigma = (6.30 \times 10^{-18} \text{ cm}^2) \times \left[1.34 \left(\frac{h\nu}{13.6 \text{ eV}} \right)^{-2.99} - 0.34 \left(\frac{h\nu}{13.6 \text{ eV}} \right)^{-3.99} \right]$$

for $h\nu > 13.6 \text{ eV}$. (29)

The photoionization rate $\zeta_{\text{H}}^{(\text{pi})}$ averaged over the shell is evaluated using equation (10).

4.8. $\text{He} + h\nu \rightarrow \text{He}^+ + e^-$ and $\text{He}^+ + h\nu \rightarrow \text{He}^{2+} + e^-$

The cross sections for photoionization of He and He^+ are (Osterbrock 1989)

$$\sigma = (7.83 \times 10^{-18} \text{ cm}^2) \times \left[1.66 \left(\frac{h\nu}{24.6 \text{ eV}} \right)^{-2.05} - 0.66 \left(\frac{h\nu}{24.6 \text{ eV}} \right)^{-3.05} \right]$$

for $h\nu > 24.6 \text{ eV}$, (30)

$$\sigma = (1.58 \times 10^{-18} \text{ cm}^2) \times \left[1.34 \left(\frac{h\nu}{54.4 \text{ eV}} \right)^{-2.99} - 0.34 \left(\frac{h\nu}{54.4 \text{ eV}} \right)^{-3.99} \right]$$

for $h\nu > 54.4 \text{ eV}$. (31)

The photoionization rates $\zeta_{\text{He}}^{(\text{pi})}$ and $\zeta_{\text{He}^+}^{(\text{pi})}$ averaged over the shell are evaluated using equation (10).

5. PHOTOCHEMICAL EVOLUTION

5.1. Initial Conditions

As initial conditions, we take He to be neutral, and 100% of the hydrogen to be in H_2 , divided equally between the first two rotation levels:

$$2 \frac{n(\text{H}_2(v=0, J=0))}{n_{\text{H}}} = 2 \frac{n(\text{H}_2(v=0, J=1))}{n_{\text{H}}} = 0.5.$$

(32)

We assume that dust grains of initial radius $a_i = 3 \times 10^{-5} \text{ cm}$ initially contribute a mass equal to 1% of the H mass, with initial number density

$$n_d = \frac{0.01 n_{\text{H}} m_{\text{H}}}{(4\pi/3)\rho a_i^3},$$

(33)

where $\rho \approx 2 \text{ g cm}^{-3}$ is the assumed density of the grain material, n_{H} is the number density of H nuclei, and m_{H} is the mass of one H atom. Thus, the initial geometric cross section per H atom is

$$\frac{n_d}{n_{\text{H}}} \pi a^2 = 2.1 \times 10^{-22} \text{ cm}^2 \text{ H}^{-1}.$$

(34)

Since the radiation propagates only in the outward direction (we are neglecting scattered light), the time evolution of each shell depends only on interior shells. We therefore calculate the complete time evolution for each shell, beginning with the first shell and proceeding outward. For each shell j , we begin integrating at retarded time $t_r = 0$. For each value of t_r , we use stored information for interior shells $i < j$ to compute the time- and frequency-dependent optical depth τ_{j-1} due to material interior to shell j .

The calculation for shell j is terminated when $t_r > 100t_0 = 10^3 \text{ s}$ (see eq. [1]) and nearly all of the flash energy has been expended, or if all of the following conditions are fulfilled: (1) all H_2 has been photodissociated to 2H and then photoionized into 2H^+ or photoionized first to H_2^+ and then to 2H^+ [our criteria for this are $\sum_i p_i(v_i, J_i) < 10^{-6}$, $x(\text{H}) < 10^{-6}$, and $x(\text{H}_2^+) < 10^{-6}$]; (2) the dust has been destroyed ($a = 0$); and (3) helium is fully photoionized to He^{2+} .

5.2. Integration Scheme

A very simple explicit scheme is used to advance the abundances in each shell:

$$y(t + \Delta t) = y(t) + (dy/dt)_t \Delta t,$$

(35)

where y is a , $n(\text{H})$, $n(\text{H}^+)$, $n(\text{He}^0)$, $n(\text{He}^+)$, $n(\text{He}^{2+})$, or H_2 vibration-rotation level population p_i .

For all cases, we used radial zone thickness $\Delta R = 6 \times 10^{16} \text{ cm}$. At a given distance r and retarded time t_r , we take the time step Δt to be

$$\Delta t = \min[\epsilon_d t_d, \epsilon_p t_p],$$

(36)

$$t_d^{-1} = \max[-T_{ii}, \zeta_{\text{H}}^{(\text{pi})}, (\zeta_{\text{H}_2^+}^{(\text{pi})} + \zeta_{\text{H}_2^+}^{(\text{pd})}), \zeta_{\text{He}}^{(\text{pi})}, \zeta_{\text{He}^+}^{(\text{pi})}],$$

(37)

$$t_p^{-1} = \zeta_{\text{H}_2}^{(\text{pi})} \frac{n(\text{H}_2)}{n(\text{H}_2^+)};$$

(38)

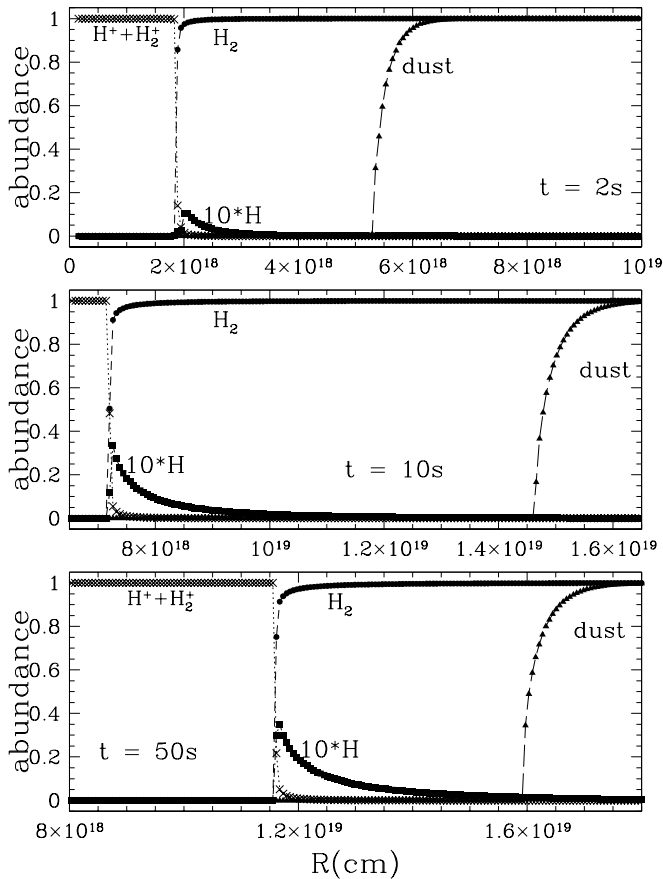


FIG. 3.—Snapshots of the ionization/dissociation/dust-destruction fronts at three values of the retarded time t_r for our adopted GRB optical transient ($L_\nu \propto \nu^{-1/2}$, given by eq. [1] with $L_0 = 2.5 \times 10^{48}$ ergs s^{-1} , $t_0 = 10$ s, and $\beta = -0.5$) in a cloud with $n_H = 10^3$ cm^{-3} . *Triangles*: Plot of dust mass $(a/a_i)^3$. *Circles*: Plot of $2n(H_2)/n_H$. *Squares*: Plot of $10 \times n(H)/n_H$. *Crosses*: Plot of $n(H^+)n(H_2^+)/n_H$. Note that different panels have different horizontal scales.

t_d is the shortest timescale for destruction, while t_p is the timescale for production of H_2^+ . The rates T_{ii} are given by equation (23). We used $(\epsilon_d, \epsilon_p) = (0.2, 0.2)$ for all cases; we verified that the computed results were insensitive to factor of 2 variations in ϵ_d and ϵ_p .

6. RESULTS

Radial abundance profiles are shown in Figure 3 for three values of the retarded time t_r , for an optical transient with the light curve given by equation (1) with spectral index $\beta = -0.5$, located in a molecular cloud of density $n_H = 10^3$ cm^{-3} .

In Figure 4 we show abundance profiles for the same three values of retarded time, for the same optical transient but situated in a cloud of density $n_H = 10^4$ cm^{-3} . In its initial molecular form, an individual shell is opaque to ionizing radiation $h\nu \lesssim 70$ eV and is highly opaque in individual H_2 resonance lines; it is therefore essential to use the shell-averaged rates given by equation (10) for continuum absorption, or equation (16) for line absorption. As one would expect, the increased opacity of the medium delays propagation of the destruction fronts.

In Figures 5 and 6 we show the locations of the dust-destruction, dissociation, and ionization fronts as functions of time for our standard optical transient in clouds of den-

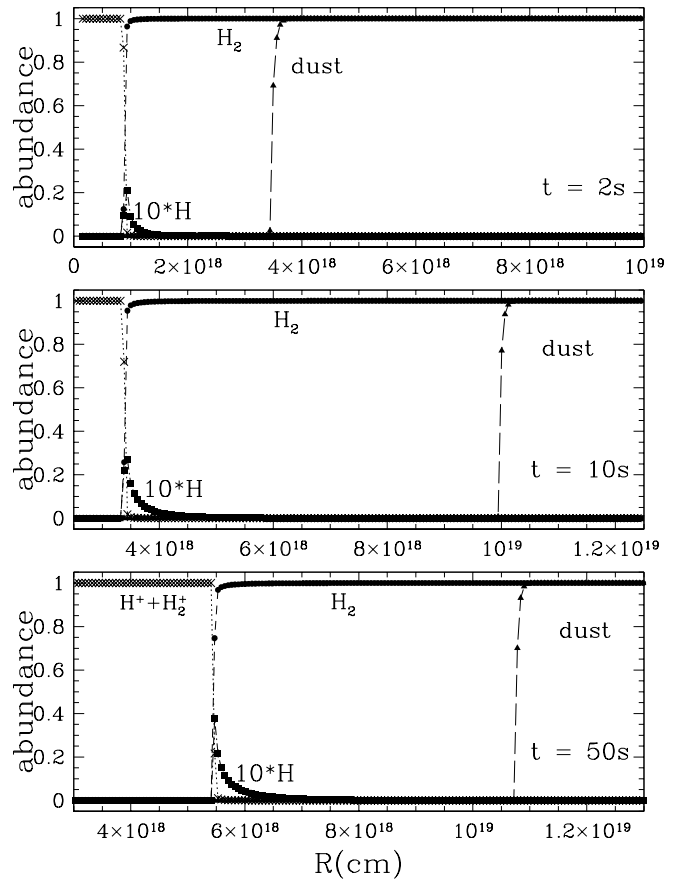


FIG. 4.—Same as Fig. 3, but for $n_H = 10^4$ cm^{-3}

sity $n_H = 10^3$ and 10^4 cm^{-3} , and we also show the front locations as functions of time for a GRB with a softer UV spectrum characterized by $\beta = -1$.

6.1. Dust Destruction

In Figure 3 we see that by $t_r = 2$ s, the dust-destruction front has already reached $R \approx 5.5 \times 10^{18}$ cm, significantly ahead of the ionization/dissociation front at $\sim 1.9 \times 10^{18}$ cm. At late times, the dust-destruction front “stalls” when the transient luminosity has dropped to the point at which it can no longer heat dust at this distance to the $T \approx 3000$ K temperatures required for significant sublimation, while the ionization/dissociation front continues to advance at a rate proportional to the luminosity. For this case ($n_H = 10^3$ cm^{-3}), the dust-destruction front (see Fig. 3) has a thickness $\delta R \approx 1 \times 10^{18}$ cm, corresponding to a gas column density $\sim 10^{21}$ cm^{-2} and an optical-UV extinction (prior to dust destruction) ~ 0.4 .

In Figures 5 and 6 we show the location of the dust-destruction front as a function of retarded time t_r for our adopted optical transient (for spectral indices $\beta = -1$ and -0.5) and cloud densities $n_H = 10^3$ and 10^4 cm^{-3} . For both cases, we confirm the conclusion of WD00: the dust-destruction front initially advances well ahead of the ionization/dissociation front, with the dust heated primarily by $h\nu \lesssim 11$ eV radiation that is not absorbed by H, He, or $H_2(v=0)$. For $n_H = 10^3$ cm^{-3} and $\beta = -0.5$, the dust-destruction radius $R_d \approx 1.6 \times 10^{19}$ cm for our adopted optical transient, while for 10^4 cm^{-3} , we find $R_d \approx 1.1 \times 10^{18}$ cm.

WD00 discussed the effects of an optical transient with peak luminosity 3×10^{48} ergs s^{-1} in 1–7 eV photons—close

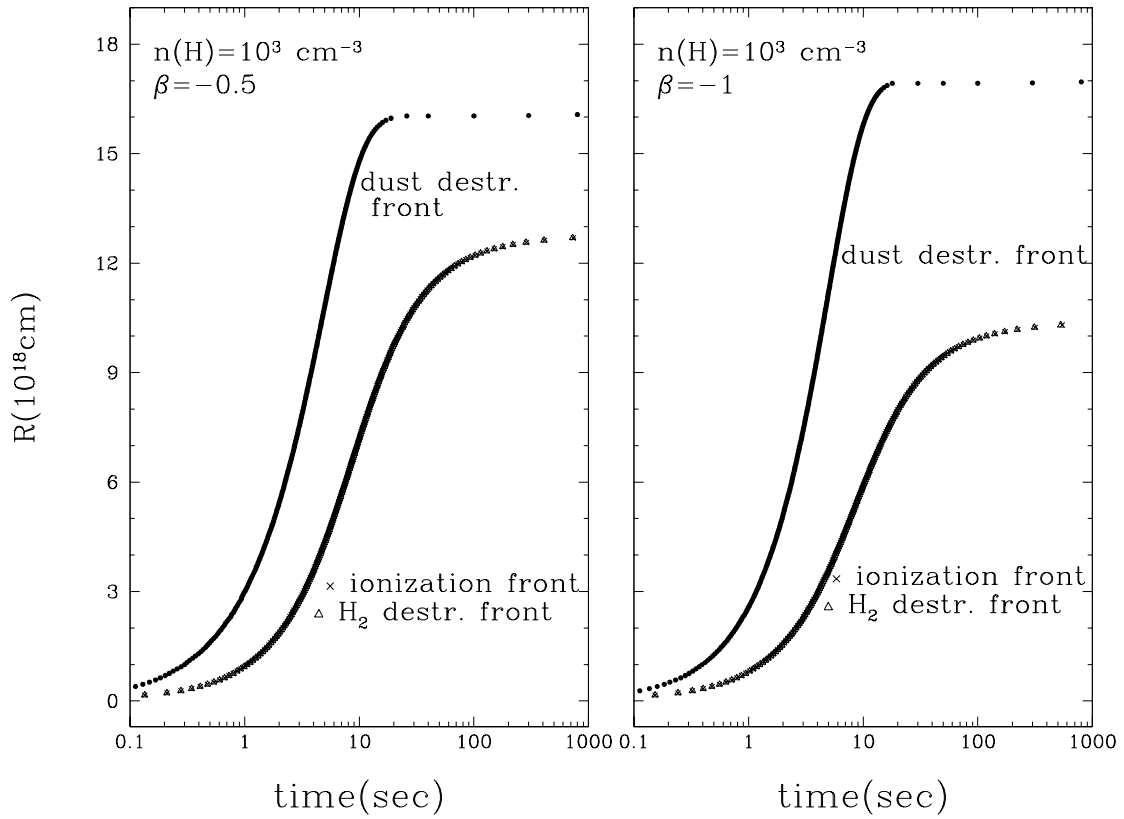


FIG. 5.—Location of the dust-destruction front, H₂-destruction front, and ionization front as functions of time for our model optical transient in molecular gas with $n_{\text{H}} = 10^3 \text{ cm}^{-3}$, for $\beta = -0.5$ and -1 . The ionization front and H₂-destruction front are nearly coincident.

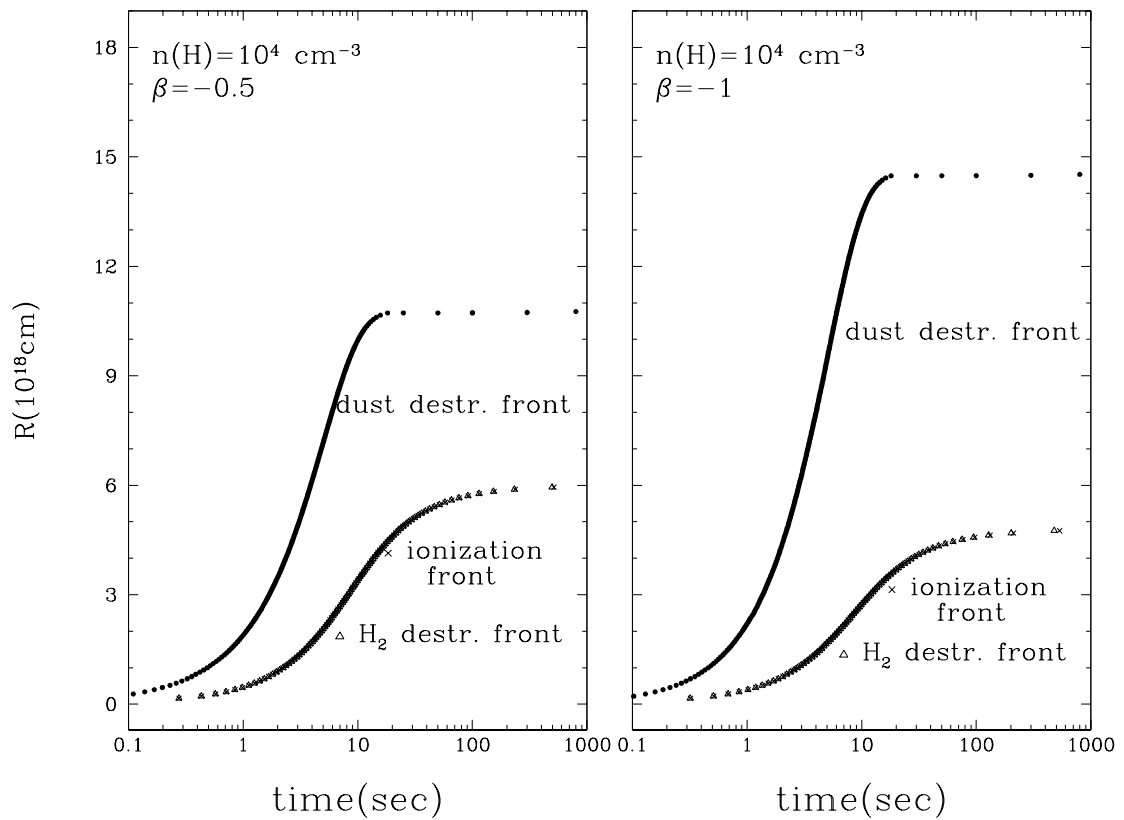


FIG. 6.—As in Fig. 5, but for cloud density $n_{\text{H}} = 10^4 \text{ cm}^{-3}$

to the peak 1–7.5 eV luminosity 2.4×10^{48} ergs s⁻¹ for our adopted light curve with $\beta = -0.5$ —and estimated the grain-destruction radius to be $R_d \approx 1.4 \times 10^{19}$ cm for $n_H \lesssim 10^3$ cm⁻³ and 1.3×10^{19} cm for $n_H = 10^4$ cm⁻³. The grain-destruction radii estimated by WD00 for these two cases are in good agreement with our detailed modeling.

6.2. Photodissociation and Photoionization

In Figure 3 we can see that the dissociation front and ionization front are merged (i.e., they do not separate). However, the ionization front is relatively sharp (with the fractional ionization varying from 0.1 to 0.9 over a column density $\Delta N_H \approx 10^{18}$ cm⁻²), whereas the dissociation front (zone where H atoms are present) tends to be broader and to extend ahead of the ionization front. For $n_H = 10^3$ cm⁻³ (see Fig. 3), the dissociation front extends $\sim 1 \times 10^{17}$ cm, corresponding to the column density $n_H \delta R \approx 10^{20}$ cm⁻³ required for H₂ to absorb most of the photons between 11.1 and 13.6 eV (Draine & Bertoldi 1996). As expected, the ionization front is unresolved, since the column density of a single shell (6×10^{19} cm⁻²) corresponds to an optical depth of ~ 380 at the Lyman edge (hence, the importance of using eq. [10] to obtain the average rate of photoionization in an optically thick shell). This is even more pronounced for the $n_H = 10^4$ cm⁻³ case, for which we have used the same shell thickness $\Delta R = 6 \times 10^{16}$ cm as for $n_H = 10^3$ cm⁻³.

6.3. Vibrationally Excited H₂

Following absorption of a Lyman or Werner band photon, about 85% of the time an H₂ molecule will undergo a spontaneous radiative decay (in $\sim 10^{-9}$ s) to a vibrationally excited level of the ground electronic state. The vibrationally excited H₂ will persist until it is either photoionized or absorbs another Lyman or Werner band photon (on the $\sim 10^3$ s timescales of interest here, spontaneous emission in the quadrupole lines is negligible, as are collisional processes). In Figure 7 we show the column density $N(\text{H}_2^*)$ of vibrationally excited H₂ as a function of time. For all cases considered, $N(\text{H}_2^*)$ increases until the UV irradiation ceases [unlike the H_2^+ , which quickly stabilizes at a value $N(\text{H}_2^+) \approx 10^{16.7}$ cm⁻²]. Photoionization acts to reduce the amount of vibrationally excited H₂ present at any instant, so GRBs with softer UV-EUV spectra would be expected to have larger column densities of vibrationally excited H₂. Our calculations confirm this: Figure 7 shows that an optical transient with spectral index $\beta = -1$ (i.e., $L_\nu \propto \nu^{-1}$) produces more vibrationally excited H₂ than a burst with $\beta = -0.5$.

As we see below, the large column densities of vibrationally excited H₂ will produce strong absorption lines.

6.4. Emergent Spectrum

The radiation reaching us from the optical transient is filtered through the dust and gas. Unless and until the photoionization front reaches the edge of the gas cloud, photoelectric absorption by H will impose a cutoff at 13.6 eV, with photoelectric absorption by H₂ further contributing to absorption above 15.4 eV. At X-ray energies $h\nu \gtrsim 10$ keV, the gas cloud may again become transparent, allowing the X-ray flash and afterglow to be observed, but our attention here is limited to energies $h\nu < 13.6$ eV, where there are four main contributions to absorption: dust, the Lyman and

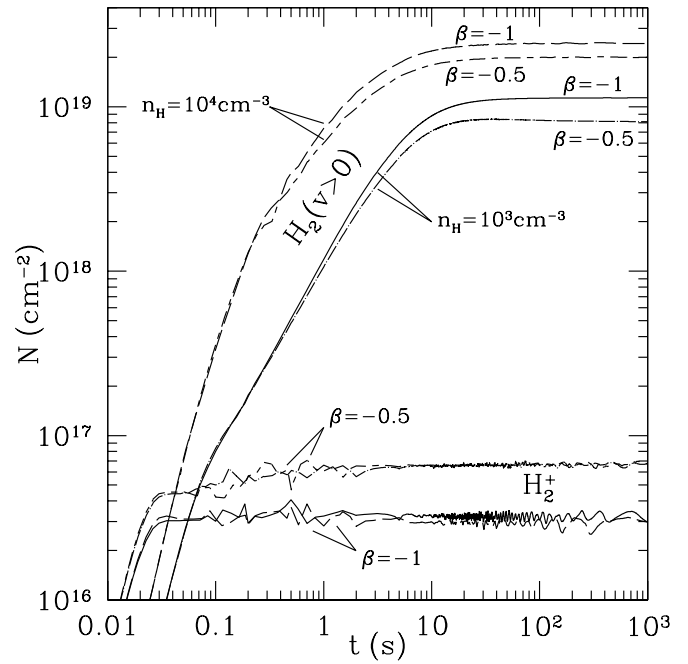


FIG. 7.—Column densities of H_2^+ and vibrationally excited H_2 for $n_H = 10^3$ and 10^4 cm⁻³, and $\beta = -1$ and -0.5 . The oscillations in $N(\text{H}_2^+)$ are due to inaccuracies in the numerical method as the ionization front traverses a radial zone. The column density of H_2^+ quickly saturates at $\sim 5 \times 10^{16}$ cm⁻², but the column density of vibrationally excited H_2 continues to rise until the ultraviolet flash fades.

Werner bands of H₂, the photodissociation of H_2^+ , and the Lyman lines of H.

The extinction by dust will affect whether the optical transient is observable. For purposes of discussion, we focus on our standard light curve with $\beta = -0.5$ in a cloud of density $n_H = 10^3$ cm⁻³. In Figure 8 we show the emergent luminos-

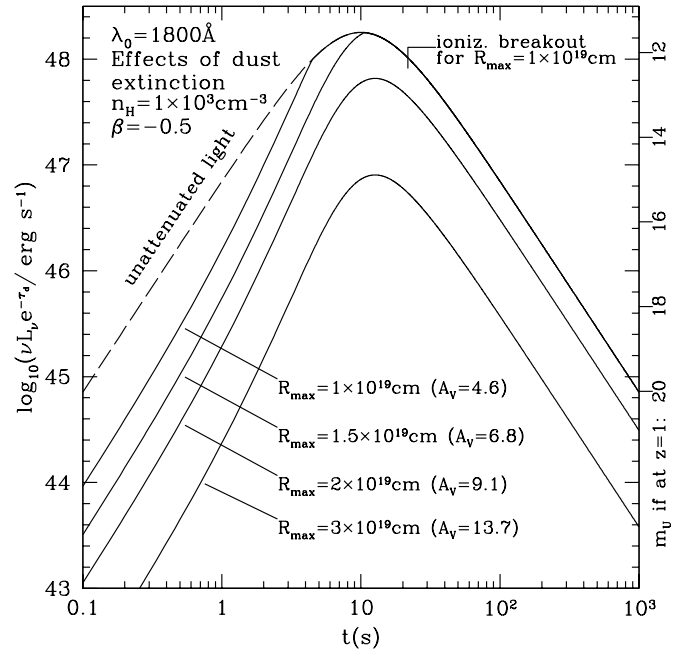


FIG. 8.—Dust-attenuated light curves at rest wavelength $\lambda_0 = 1800$ Å for different values of the cloud radius R_{max} , for a GRB with $\beta = -0.5$ in a cloud with $n_H = 10^3$ cm⁻³. A dust extinction cross section per nucleon of 4.2×10^{-22} cm² is assumed. For a GRB at $z = 1$, the U band apparent magnitude scale is indicated on the right.

ity at rest wavelength $\lambda = 1800 \text{ \AA}$ after extinction by dust. Light curves are shown for various assumed cloud radii; for each case, the initial visual extinction A_V to the GRB is indicated. In the case of an $R = 1 \times 10^{19} \text{ cm}$ cloud radius, the ionization/dissociation front reaches the cloud surface at $t \approx 22 \text{ s}$; after this time, there will of course no longer be absorption features of H_2 appearing in the spectrum of the GRB. For $R > 1.3 \times 10^{19} \text{ cm}$, however, the ionization/dissociation front is contained within the cloud, and the H_2 absorption lines will persist in the spectrum of the GRB afterglow at late times. Note in Figure 8 that for $R = 1.5 \times 10^{19} \text{ cm}$, the dust-destruction front reaches the cloud surface at $t_r = 11 \text{ s}$, after which the light curve is unattenuated by dust.

By destroying the dust out to $1.6 \times 10^{19} \text{ cm}$, the GRB has reduced the extinction between us and the GRB by $\Delta A \approx 7.3 \text{ mag}$. Thus, if, for example, the dust in the cloud had initially presented an extinction of 10 mag to the GRB, the GRB afterglow would be subject to only 2.7 mag of foreground dust.

The H_2^+ column densities tend to be considerably smaller than those of H_2 (see Fig. 7), so we have not attempted to calculate the column densities of the individual vibration-rotation levels and the $X^2\Sigma_g^+ \rightarrow C^2\Pi_u$ ultraviolet absorption lines out of these levels. Most of the electronic absorption by H_2^+ will be in $X^2\Sigma_g^+ \rightarrow A^2\Sigma_u^+$ photodissociating transitions, which contribute continuous absorption that we have approximated by equation (27).

In Figure 9 we show the transmission of the foreground medium for the $n_{\text{H}} = 10^3 \text{ cm}^{-3}$ cloud and spectral index $\beta = -0.5$, for the spectral resolution $R = 350$ characteristic of the grism on the *Swift* Ultraviolet/Optical Telescope (UVOT). Figure 9 shows *only* the absorption due to lines of H_2 and H and the continuous absorption of H_2^+ . Voigt profiles were used for both the H and H_2 lines. Over the $\lesssim 10^3 \text{ s}$ timescales of interest here, the H and H_2 gas is essentially collisionless. For the H_2 lines, we have therefore used a Doppler broadening parameter $b = 3 \text{ km s}^{-1}$ characteristic

of “microturbulence” in the quiescent pre-GRB molecular gas. The H atoms, on the other hand, will have a velocity distribution resulting from the photodissociation of H_2 and H_2^+ . The mean kinetic energy per H atom is $\sim 0.15 \text{ eV}$ (Stephens & Dalgarno 1973), corresponding to a Maxwellian distribution with $b \approx 4 \text{ km s}^{-1}$; this will add in quadrature to the microturbulence, so we take $b = 5 \text{ km s}^{-1}$ for the H atoms.

The spectrum consists of literally thousands of saturated narrow lines, but even at $R = 350$ resolution, a number of absorption features are conspicuous. In Figure 9 we have labeled 32 conspicuous features longward of $\lambda = 1111 \text{ \AA}$. These features are all blends of a number of nearby lines. For each feature in Table 1, we list the three strongest lines within $\pm\lambda/(2R) = \pm 1.3 \times 10^{-3}\lambda$ of the central wavelength of each feature. The strongest lines tend to be saturated [e.g., the strongest line in the conspicuous 1277.3 \AA feature is Lyman 8–6 $R(1)$ 1277.39 \AA , with a central optical depth $\tau_0 = 1150$ and an equivalent width $W_\lambda/\lambda = 8.3 \times 10^{-4}$].

Figure 10 shows the transmission spectrum observed with three different spectral resolutions: $R = 100, 350$, and 1000 . While the $R = 1000$ spectrum of course shows the most structure, we see that the $R = 350$ resolution is quite well matched to the widths of the prominent absorption blends. If the resolution is degraded to $R = 100$, most of the absorption blends still appear as well-defined minima, although a few do not (e.g., $\lambda = 1621.7 \text{ \AA}$). For $R = 100$ observations, it would appear that a signal-to-noise ratio of 10 would suffice to test for the presence or absence of the stronger absorption features (e.g., $1607.0, 1460.0, 1401.9, 1277.3$, and 1254.8 \AA).

Because the lines are saturated, the overall spectrum is not sensitive to the precise amount of vibrationally excited H_2 . To see this, in Figure 11 we show the $R = 350$ spectrum for three different values of the column density $N(\text{H}_2^*)$ of vibrationally excited H_2 , ranging from $N(\text{H}_2^*) = 10^{18.35} \text{ cm}^{-2}$ (the value at $t = 2 \text{ s}$ for the $\beta = -0.5, n_{\text{H}} = 10^3 \text{ cm}^{-3}$ case) to $N(\text{H}_2^*) = 10^{19.30} \text{ cm}^{-2}$ (the value at $t = 10^3 \text{ s}$ for the $\beta = -0.5, n_{\text{H}} = 10^4 \text{ cm}^{-3}$ case). While the depth of the absorption features does increase with increasing $N(\text{H}_2^*)$, the increase is fairly modest despite the order-of-magnitude change in $N(\text{H}_2^*)$.

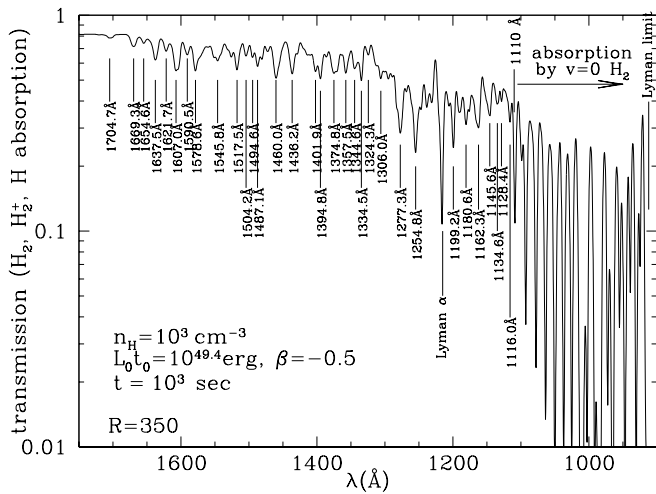


Fig. 9.—Transmission spectrum of the intervening H_2 , H, and H_2^+ at $t = 10^3 \text{ s}$, for a GRB in a cloud with $n_{\text{H}} = 10^3 \text{ cm}^{-3}$, as observed by a spectrograph with $R = \lambda/\text{FWHM}_\lambda = 350$. The GRB is assumed to have a spectrum with $\beta = -0.5$ (i.e., $L_\nu \propto \nu^{-0.5}$). Continuum absorption by dust contributes additional attenuation. At resolution $R = 350$, a number of $\lambda > 1110 \text{ \AA}$ absorption “features” from vibrationally excited H_2 are evident and are labeled by wavelength. Some of the stronger lines contributing to these features are listed in Table 1.

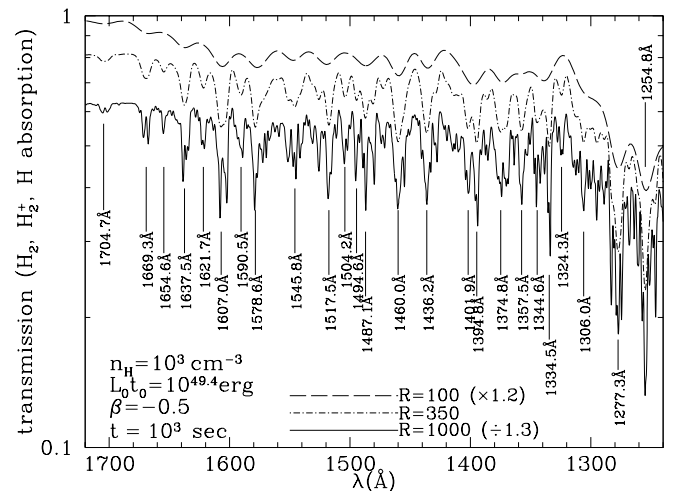


Fig. 10.—Plot of $1240\text{--}1720 \text{ \AA}$ transmission spectrum for the same conditions as Fig. 9 at spectral resolutions $R = 100, 350$, and 1000 . Note that the $R = 100$ and $R = 1000$ spectra have been offset for clarity.

TABLE 1
 $\lambda > 1110 \text{ \AA}$ ABSORPTION FEATURES FROM UV-PUMPED H_2

$\lambda^a(\text{\AA})$	THREE STRONGEST CONTRIBUTING LINES ^b (\AA)		
	(1)	(2)	(3)
1704.7	3–13 <i>P</i> (1) 1704.51	3–13 <i>R</i> (0) 1702.63	3–13 <i>P</i> (2) 1705.29
1669.3	2–11 <i>R</i> (1) 1667.46	4–13 <i>R</i> (1) 1667.28	2–11 <i>P</i> (1) 1670.40
1654.6	1–10 <i>R</i> (1) 1654.99	5–14 <i>P</i> (1) 1654.19	1–10 <i>R</i> (0) 1655.40
1637.5	4–12 <i>R</i> (1) 1638.90	3–11 <i>P</i> (1) 1636.33	4–12 <i>R</i> (2) 1638.52
1621.7	2–10 <i>R</i> (1) 1620.74	2–10 <i>P</i> (1) 1623.51	2–10 <i>R</i> (0) 1621.05
1607.0	6–13 <i>P</i> (1) 1607.50	5–12 <i>R</i> (0) 1608.43	5–12 <i>R</i> (3) 1607.58
1590.5	3–10 <i>R</i> (1) 1588.76	3–10 <i>P</i> (1) 1591.31	3–10 <i>R</i> (0) 1588.98
1578.6	7–13 <i>R</i> (1) 1577.02	0–8 <i>R</i> (1) 1576.88	7–13 <i>P</i> (1) 1579.18
1545.8	1–8 <i>R</i> (1) 1544.90	1–8 <i>P</i> (1) 1547.54	1–8 <i>R</i> (0) 1544.94
1517.5	0–7 <i>R</i> (1) 1516.23	2–8 <i>P</i> (1) 1517.44	0–7 <i>P</i> (1) 1518.90
1504.2	10–13 <i>P</i> (1) 1504.15	10–13 <i>P</i> (2) 1504.92	9–12 <i>P</i> (1) 1503.78
1494.6	1–7 <i>P</i> (2) 1491.71	1–7 <i>P</i> (3) 1495.22	11–14 <i>R</i> (1) 1493.83
1487.1	1–7 <i>R</i> (1) 1486.63	1–7 <i>P</i> (1) 1489.08	1–7 <i>R</i> (0) 1486.53
1460.0	0–6 <i>P</i> (2) 1460.17	4–8 <i>R</i> (1) 1460.77	0–6 <i>R</i> (3) 1458.14
1436.2	3–7 <i>P</i> (1) 1435.05	5–8 <i>R</i> (1) 1436.09	5–8 <i>P</i> (1) 1438.02
1401.9	2–6 <i>R</i> (1) 1402.14	0–5 <i>P</i> (3) 1402.66	2–6 <i>R</i> (0) 1401.87
1394.8	0–5 <i>R</i> (1) 1393.97	0–5 <i>P</i> (1) 1396.23	0–5 <i>R</i> (0) 1393.73
1374.8	10–9 <i>R</i> (1) 1374.49	1–5 <i>P</i> (2) 1373.66	10–9 <i>P</i> (1) 1375.98
1357.5	4–6 <i>R</i> (1) 1355.56	4–6 <i>R</i> (2) 1357.35	4–6 <i>R</i> (2) 1356.85
1344.6	2–5 <i>R</i> (1) 1345.40	2–5 <i>R</i> (0) 1345.04	7–7 <i>R</i> (1) 1343.60
1334.5	0–4 <i>R</i> (1) 1333.80	0–4 <i>R</i> (0) 1333.48	0–4 <i>P</i> (1) 1335.87
1324.3	3–5 <i>R</i> (1) 1323.28	3–5 <i>R</i> (0) 1322.80	3–5 <i>P</i> (1) 1325.06
1306.0	9–7 <i>R</i> (1) 1306.21	3–9 <i>R</i> (1) 1305.59	9–7 <i>P</i> (1) 1307.58
1277.3	0–3 <i>P</i> (1) 1276.82	0–3 <i>R</i> (2) 1276.33	0–3 <i>R</i> (3) 1278.74
1254.8	1–3 <i>R</i> (1) 1253.94	1–3 <i>R</i> (0) 1253.50	1–3 <i>P</i> (1) 1255.68
1199.2	1–2 <i>R</i> (1) 1198.49	1–2 <i>R</i> (0) 1198.01	1–2 <i>P</i> (1) 1200.08
1180.6	2–2 <i>R</i> (1) 1180.42	2–2 <i>P</i> (1) 1181.89	2–2 <i>R</i> (2) 1181.93
1162.3	1–4 <i>Q</i> (1) 1161.29 ^c	0–1 <i>R</i> (1) 1162.17	3–2 <i>R</i> (1) 1163.37
1145.6	1–1 <i>R</i> (1) 1144.71	0–3 <i>Q</i> (1) 1145.90 ^c	1–1 <i>P</i> (1) 1146.16
1134.6	2–1 <i>P</i> (3) 1135.36	2–4 <i>Q</i> (2) 1133.77 ^c	15–5 <i>R</i> (1) 1136.12
1128.4	2–1 <i>R</i> (1) 1128.22	2–1 <i>R</i> (0) 1127.68	2–1 <i>R</i> (2) 1129.74
1116.0	1–3 <i>Q</i> (1) 1116.51 ^c	1–3 <i>R</i> (1) 1114.93 ^c	3–1 <i>R</i> (3) 1116.66

^a Wavelength of transmission minimum at resolution $R = 350$.

^b All transitions are Lyman band unless otherwise indicated.

^c Werner band transition.

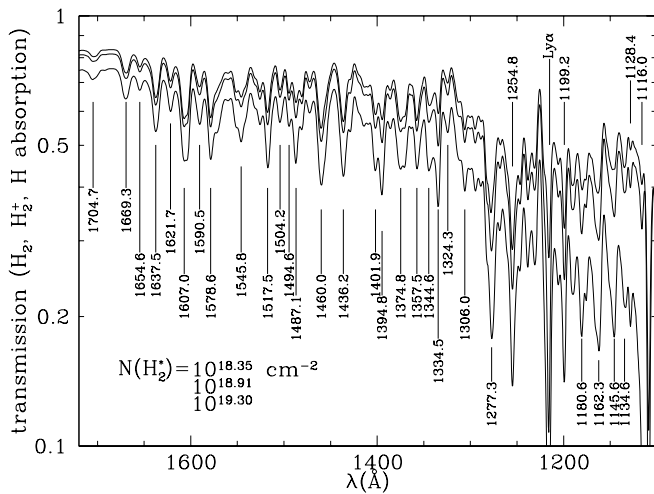


FIG. 11.—Plot of 1100–1720 \AA transmission spectrum for $N(\text{H}_2^*) = 10^{18.35}$, $10^{18.91}$, and $10^{19.30} \text{ cm}^{-2}$, at spectral resolution $R = 350$. The absorption feature strengths are nearly unchanged because of saturation of the H_2 absorption lines.

7. OBSERVATIONAL PROSPECTS: *HETE* AND *SWIFT*

The presence or absence of the absorption features in Table 1 will indicate whether or not GRBs occur in the vicinity of molecular gas. The present paper has carried out simulations of the effect that the optical and ultraviolet radiation from a GRB will have on nearby gas and dust, assuming that the GRB progenitor is located in a uniform molecular medium of density $n_{\text{H}} = 10^3$ or 10^4 cm^{-3} . It is important to realize, however, that vibrationally excited H_2 can be produced even if the GRB is in a low-density region, but there is molecular gas on the line of sight close enough to the GRB to be optically pumped by the UV radiation. Absorption features will be conspicuous for vibrationally excited H_2 column densities $N(\text{H}_2^*) > 10^{18} \text{ cm}^{-2}$. This will be produced provided the total H_2 column exceeds 10^{21} cm^{-2} and the GRB flash includes a fluence per logarithmic interval $F_{1000 \text{ \AA}} = (1/4\pi R^2) \int dt [\nu L_\nu / (h\nu)]_{1000 \text{ \AA}} > F_{\text{min}}$, where $F_{\text{min}} \approx 5 \times 10^{18} \text{ cm}^{-2}$ of photons at $\lambda \approx 1000 \text{ \AA}$. For the light curve in equation (1), this fluence occurs at a distance

$$R < \left(\frac{L_0 t_0}{2F_{\text{min}} I_{\text{H}}} \right)^{1/2} \left(\frac{12.4}{13.6} \right)^{\beta/2} \approx 110 \text{ pc}, \quad (39)$$

where we have taken $L_0 t_0 = 2.5 \times 10^{49}$ ergs and $\beta = -0.5$. Therefore, even if the GRB occurs in a low-density region, absorption by vibrationally excited H_2 may be observable if there is a molecular cloud on the line of sight within ~ 100 pc of the GRB.

Early detection and accurate positions for GRBs may enable spectroscopic observations to be carried out while the fireball/afterglow is still bright. The *High Energy Transient Explorer (HETE)* is intended to provide rapid positions to enable early ground-based observations. This may allow ground-based telescopes to obtain $R > 100$ spectra of the afterglow for afterglows at $z > 1.25$, where the $\lambda = 1600$ Å region is redshifted into the U band. For redshift $2.2 < z < 4.3$, the entire 1110–1705 Å spectrum would be observable from the ground with silicon CCD detectors.

The *Swift* Gamma Ray Burst Explorer mission, scheduled to be launched in 2003, is expected to return positions within seconds for ~ 1000 GRBs over its 3 year mission. The UVOT on *Swift* will image ~ 300 GRBs within 70 s of the burst, with 6500–1700 Å wavelength coverage. For the brightest bursts, observations through a grism can be made, yielding an $R \approx 200$ –400 spectrum over the 6500–1700 Å spectral range (Roming 2001).² The UV sensitivity means that rest wavelengths of 1705–1600 Å (a range that includes six of the absorption features in Table 1) could be observed for GRBs at redshifts $z > 0.06$. For GRBs at $0.53 < z < 2.81$, the UVOT spectral range will include the entire 1705–1110 Å range, in which absorption lines from vibrationally excited H_2 are conspicuous.

8. SUMMARY

The luminous optical transient associated with at least some GRBs will have drastic effects on surrounding molecular gas and dust if the GRB is situated within a molecular cloud. To illustrate the effects, we have adopted a provi-

sional light curve for a GRB optical transient and have considered power-law spectra $L_\nu \propto \nu^{-0.5}$ and $L_\nu \propto \nu^{-1}$. We have calculated the resulting photoionization and photodissociation of the surrounding gas and thermal sublimation of the dust for two values of the gas density, $n_H = 10^3$ and 10^4 cm^{-3} . Our principal results are as follows:

1. Dust will be destroyed out to distances $R_d \approx 10^{19}$ cm in clouds of density $n_H \lesssim 10^4$ cm^{-3} , confirming earlier estimates by WD00.
2. The ionization and dissociation fronts are merged for spectra $L_\nu \propto \nu^{-0.5}$ and $\propto \nu^{-1}$. The destruction of the H_2 is therefore due in part to photodissociation and in part to photoionization.
3. As proposed by Draine (2000), a substantial column density of vibrationally excited H_2 is created as long as the ionization-dissociation front has not broken out of the molecular cloud. This vibrationally excited H_2 will produce strong absorption lines in the 1705–1110 Å region, in which $Ly\alpha$ would normally be the only strong absorption line.
4. Spectra of GRB optical transients and afterglows should be compared with the predicted absorption spectra shown in Figures 9–11. Even if the signal-to-noise ratio does not permit detection of individual features, cross-correlation may make it possible to detect the ensemble of lines between 1650 and 1110 Å. Detection of such absorption by vibrationally excited H_2 would be unequivocal evidence for association of the GRB with molecular gas. The UVOT grism on the *Swift* Gamma Ray Burst Explorer mission may be able to measure these features in the spectra of the brighter GRBs at redshift $z \gtrsim 0.1$.

We thank E. Roueff for making H_2 data available, S. Hunsberger for providing the specifications for the *Swift* UVOT instrument, J. Krolik and B. Paczyński for helpful discussions, and R. H. Lupton for availability of the SM software package. We are grateful to the anonymous referee for a careful reading of the manuscript and helpful suggestions for its improvement. This work was supported in part by NSF grant AST-9988126.

² Available at <http://www.swift.psu.edu/uvot/doc/index.html>.

REFERENCES

- Abgrall, H., Roueff, E., Launay, F., Roncin, J.-Y., & Subtil, J.-L. 1993a, *A&AS*, 101, 273
 ———. 1993b, *A&AS*, 101, 323
 Akerlof, C. W., et al. 1999, *Nature*, 398, 400
 Bates, D. R., & Öpik, U. 1968, *J. Phys. B*, 1, 543
 Böttcher, M., Dermer, C. D., & Liang, E. P. 1999, *A&AS*, 138, 543
 Draine, B. T. 2000, *ApJ*, 532, 273
 Draine, B. T., & Bertoldi, F. 1996, *ApJ*, 468, 269
 Draine, B. T., & Salpeter, E. E. 1979, *ApJ*, 231, 77
 Fruchter, A., Krolik, J. H., & Rhoads, J. E. 2001, *ApJ*, 563, 597
 Guhathakurta, P., & Draine, B. T. 1989, *ApJ*, 345, 230 (GD89)
 Habing, H. J. 1968, *Bull. Astron. Inst. Netherlands*, 19, 421
 Israel, G. L., Marconi, G., Covino, S., Lazzati, D., Ghisellini, G., Campana, S., Guzzo, L., Guerrero, G., & Stella, L. 1999, *A&A*, 348, L5
 Lazzati, D., Covino, S., & Ghisellini, G. 2002, *MNRAS*, 330, 583
 Lazzati, D., Perna, R., & Ghisellini, G. 2001, *MNRAS*, 325, L19
 Leach, C. A., & Moss, R. E. 1995, *Annu. Rev. Phys. Chem.*, 46, 55
 Lee, B. C., et al. 2001, *ApJ*, 561, 183
 MacFadyen, A. I., Woosley, S. E., & Heger, A. 2001, *ApJ*, 550, 410
 Masetti, N., et al. 2001, *A&A*, 374, 382
 Muller, E. W., & Tsong, T. T. 1969, *Field Ion Microscopy* (New York: American Elsevier)
- Osterbrock, D. E. 1989, *Astrophysics of Gaseous Nebulae* (Mill Valley: University Science Books)
 Paczyński, B. 1998, *ApJ*, 494, L45
 ———. 2001, in *Supernovae and Gamma Ray Bursts: The Greatest Explosions since the Big Bang*, ed. M. Livio, N. Panagia & K. Sahu (Cambridge: Cambridge Univ. Press), 1
 Perna, R., & Loeb, A. 1998, *ApJ*, 501, 467
 Ramirez-Ruiz, E., Trentham, W., & Blain, A. W. 2002, *MNRAS*, 329, 465
 Roming, P. 2001, *Swift* Specification for the Ultra Violet Optical Telescope, SWIFT-UVOT-002-R00, Penn State University
 Smith, R. K., & Dwek, E. 1998, *ApJ*, 503, 831
 Stanek, K. Z., Garnavich, P. M., Jha, S., Kilgard, R. E., McDowell, J. C., Bersier, D., Challis, P. M., Falco, E., & Quinn, J. L. 2001, *ApJ*, 563, 592
 Stanek, K. Z., Garnavich, P. M., Kaluzny, J., Pych, W., & Thompson, I. 1999, *ApJ*, 522, L39
 Stephens, T. L., & Dalgarno, A. 1973, *ApJ*, 186, 165
 von Busch, F., & Dunn, G. H. 1972, *Phys. Rev. A*, 5, 1726
 Waxman, E., & Draine, B. T. 2000, *ApJ*, 537, 796 (WD00)
 Williams, G. G., et al. 2000, in *AIP Conf. Proc.* 526, 5th Huntsville Symp. on Gamma-Ray Bursts, ed. R. M. Kippen, R. S. Mallozzi, & G. J. Fishman (New York: AIP), 250
 Yan, M., Sadeghpour, H. R., & Dalgarno, A. 1998, *ApJ*, 496, 1044